ELSEVIER

Journal of Biomechanics 39 (2006) 3036–3044

JOURNAL OF BIOMECHANICS

www.elsevier.com/locate/jbiomech
www.JBiomech.com

Analytical modeling of the instantaneous maximal transvalvular pressure gradient in aortic stenosis

Damien Garcia[a,*], Lyes Kadem[a], David Savéry[b], Philippe Pibarot[c], Louis-Gilles Durand[a]

[a]*Biomedical Engineering Laboratory, Clinical Research Institute of Montreal, IRCM, 110 Pine West Avenue, Montreal, QC, Canada H2W 1R7*
[b]*Philips Research USA, Healthcare Systems and Information Technology, Briarcliff Manor, NY, USA*
[c]*Research Center of Laval Hospital-Quebec Heart Institute, Laval University, Sainte-Foy, QC, Canada*

Accepted 12 October 2005

Abstract

In presence of aortic stenosis, a jet is produced downstream of the aortic valve annulus during systole. The vena contracta corresponds to the location where the cross-sectional area of the flow jet is minimal. The maximal transvalvular pressure gradient (TPG_{max}) is the difference between the static pressure in the left ventricle and that in the vena contracta. TPG_{max} is highly time-dependent over systole and is known to depend upon the transvalvular flow rate, the effective orifice area (EOA) of the aortic valve and the cross-sectional area of the left ventricular outflow tract. However, it is still unclear how these parameters modify the TPG_{max} waveform. We thus derived an explicit analytical model to describe the instantaneous TPG_{max} across the aortic valve during systole. This theoretical model was validated with in vivo experiments obtained in 19 pigs with supravalvular aortic stenosis. Instantaneous TPG_{max} was measured by catheter and its waveform was compared with the one determined from the derived equation. Our results showed a very good concordance between the measured and predicted instantaneous TPG_{max}. Total relative error and mean absolute error were on average $9.4 \pm 4.9\%$ and 2.1 ± 1.1 mmHg, respectively. The analytical model proposed and validated in this study provides new insight into the behaviour of the TPG_{max} and thus of the aortic pressure at the level of vena contracta. Because the static pressure at the coronary inlet is similar to that at the vena contracta, the proposed equation will permit to further examine the impact of aortic stenosis on coronary blood flow.

Keywords: Aortic stenosis; Heart valve; Pressure gradient; Analytical modeling; Animal data; Hemodynamics

1. Introduction

Aortic stenosis (AS) is the most frequent cause of valvular replacement in developed countries (Tornos, 2001). As the blood flow passes through an AS, it forms a jet, which contracts to a minimum cross-sectional area (so-called effective orifice area, EOA) at the level of the vena contracta (location 2, Fig. 1). The difference between the left ventricular (LV) static pressure (P_{LV}, location 1, Fig. 1) and the static pressure at the vena contracta (P_{VC}, location 2) is the maximal transvalvular pressure gradient (TPG_{max}) whereas the difference between P_{LV} and the recovered aortic pressure (P_A, location 3) is the net transvalvular pressure gradient (TPG_{net}). Using the expression of instantaneous TPG_{net}, we have developed a mathematical model (V^3 model) describing the ventricular–valvular–vascular interaction under various pathophysiologic conditions (Garcia et al., 2005a).

LV failure occurs when demand of LV myocardial oxygen exceeds supply, the latter being tightly coupled to the left coronary blood flow (Braunwald et al., 1958). The left coronary circulation is essentially determined by LV pressure and by the left coronary inlet pressure (Hoffman and Spaan, 1990). The vena contracta and the left coronary inlet are located at about the same distance

*Corresponding author. Tel.: +1 514 987 5722; fax: +1 514 987 5705.
E-mail address: damien.garcia@ircm.qc.ca (D. Garcia).

0021-9290/$ - see front matter © 2005 Elsevier Ltd. All rights reserved.
doi:10.1016/j.jbiomech.2005.10.013

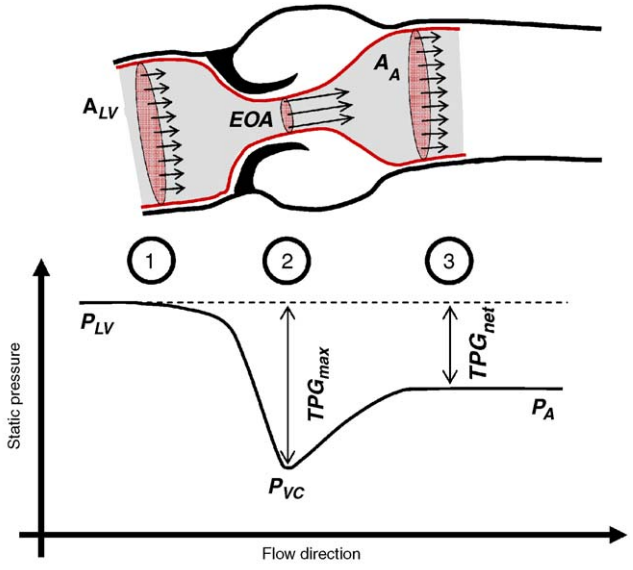

Fig. 1. Schema of the flow across an aortic stenosis during systole and corresponding pressure field along the flow axis. Locations 1, 2 and 3 correspond to the detachment of the flow from the left ventricular outflow tract, the vena contracta and the location where aortic pressure is totally recovered. TPG is the transvalvular pressure gradient and EOA is the valvular effective orifice area. P_{LV} = left ventricular pressure, P_{VC} = pressure in the vena contracta, P_A = aortic pressure, A_{LV} = cross-sectional area of the left ventricular outflow tract, A_A = aortic cross-sectional area.

downstream of the valve annulus, and it has been shown by Sung et al. (1997) that the static pressure does not change significantly from the flow axis to the wall. Thus, static pressure in the left coronary inlet is similar to that in the vena contracta (P_{VC}). Knowing the expressions of instantaneous TPG_{max} and LV pressure might thus provide the instantaneous coronary inlet pressure. This would allow us to combine the V^3 model with a lumped model of the left coronary circulation such as the one proposed by Judd and Mates (1991) and Mates and Judd (1993). Such a comprehensive model will allow studying the impact of AS on left coronary blood flow. Therefore, with this forthcoming purpose in view, the primary objective of the present study was to propose an analytical model of the instantaneous TPG_{max}. In the following sections, TPG_{max} will refer to instantaneous TPG_{max}, unless mentioned otherwise.

2. Methods: mathematical derivation of TPG_{max}

2.1. Hypotheses

Systole is defined as the period where the transvalvular flow rate $Q>0$ (LV ejection period). The flow pattern across an aortic stenosis is mainly characterized by a contraction as far as the vena contracta, followed by an abrupt expansion (Fig. 1). Within the expansion, some dynamic pressure is converted to static pressure. This process is unstable and generates turbulence, which means that a part of the initial fluid energy is irreversibly lost. On the contrary, no significant turbulence occurs upstream from the vena contracta since the conversion of static to dynamic pressure is stable and is a low-energy dissipation process (Ward-Smith, 1980). Thus, we first suppose that the fluid is ideal (i.e. incompressible and non viscous) upstream from the vena contracta. Second, we assume that the aortic valve opens and closes instantaneously and that its EOA remains constant during systole. Furthermore, we assume that the flow velocity profile is flat throughout the region of interest (shaded zone located between location 1 and location 3, Fig. 1). Finally the cross-sectional area of the LV outflow tract (LVOT, location 1) and that of the ascending aorta (location 3) are supposed invariant throughout systole. For simplicity, they are supposed similar and noted A.

2.2. Derivation of the TPG_{max}

During systole, the blood accelerates between the LVOT (location 1, Fig. 1) and the vena contracta (location 2). No significant energy loss occurs during this convective acceleration (Miller, 1996). Neglecting the effects of gravitation, the generalized Bernoulli equation used along a streamline linking location 1 with location 2 yields TPG_{max}:

$$\mathrm{TPG_{max}} = P_1 - P_2 = \frac{1}{2}\rho(V_2^2 - V_1^2) + \rho\int_1^2 \frac{\partial V}{\partial t}\,\mathrm{d}l, \quad (1)$$

where P, V, and ρ are the static pressure, the velocity and the density of the fluid, respectively. The coordinate l is the curvilinear coordinate along the streamline. Using the conservation of mass, the transvalvular flow rate Q can be written as $Q = AV_1 = \mathrm{EOA}\ V_2 = A(l)\ V(l)$, where $A(l)$ is the cross-sectional area occupied by the through-flow at the location l. If we assume that $A(l)$ is time independent, Eq. (1) becomes:

$$\mathrm{TPG_{max}} = \frac{1}{2}\rho Q^2\left(\frac{1}{\mathrm{EOA}^2} - \frac{1}{A^2}\right) + \rho\frac{\partial Q}{\partial t}\int_1^2 \frac{1}{A(l)}\,\mathrm{d}l. \quad (2)$$

Time integration of Eq. (2) over systole eliminates the time derivative of Q, which leads to the mean TPG_{max}:

$$\overline{\mathrm{TPG_{max}}} = \frac{1}{2}\rho\overline{Q^2}\left(\frac{1}{\mathrm{EOA}^2} - \frac{1}{A^2}\right), \quad (3)$$

where the overline denotes the systolic temporal mean. We now define the parameter λ^*, which is homogeneous to a length, as follows:

$$\frac{1}{\lambda^*} = \int_1^2 \frac{1}{A(l)}\,\mathrm{d}l. \quad (4)$$

To obtain the complete expression of TPG_{max}, one has to calculate $1/\lambda^*$. It can be noted that when EOA (i.e. $A(l=2)$), converges towards zero, this term tends towards $+\infty$. On the contrary, when the stenosis becomes less and less severe, converging towards a no-stenotic case, location 2 tends towards location 1. Hence, if $EOA = A$ (no stenosis), $1/\lambda^*$ is zero and $TPG_{max} = 0$. The upstream flow geometry depends mainly upon EOA and A (Gurevich, 1965; Ward-Smith, 1980) so that a dimensional analysis gives the following relation linking $1/\lambda^*$ with EOA/A:

$$\frac{\sqrt{A}}{\lambda^*} = f\left(\frac{A}{EOA}\right). \tag{5}$$

A simple type of functions f defined on $[1, +\infty[$ that meets the two aforementioned boundary conditions (i.e. $f(x) \to +\infty$ when $x \to +\infty$ and $f(1) = 0$) is the following:

$$\frac{\sqrt{A}}{\lambda^*} = \alpha\left[\left(\frac{A}{EOA}\right)^{\beta} - 1\right]^{\gamma}, \tag{6}$$

where α, β and γ are three strictly positive constants to be solved. Consequently, from Eqs. (2), (4) and (6), the expression of TPG_{max} becomes:

$$TPG_{max} = \frac{1}{2}\rho Q^2\left(\frac{1}{EOA^2} - \frac{1}{A^2}\right) + \rho\alpha\frac{1}{\sqrt{A}}\frac{\partial Q}{\partial t}\left[\left(\frac{A}{EOA}\right)^{\beta} - 1\right]^{\gamma}. \tag{7}$$

The constants present in Eq. (7) were determined analytically as described below.

2.3. Determination of the three constants

We note L_{23} the recovery length that is the distance separating the vena contracta from the location beyond where static pressure is totally recovered. To determine α, β and γ, one will study the behaviour of L_{23}. According to our previous study (see Eq. (10) in (Garcia et al., 2005b)), L_{23} is related to $1/\lambda^*$ as follows:

$$\frac{L_{23}}{A} = 2\pi\sqrt{\frac{1}{EOA} - \frac{1}{A}} - \frac{1}{\lambda^*} \tag{8}$$

and more precisely, it follows from Eq. (6) that:

$$\frac{L_{23}}{\sqrt{A}} = 2\pi\sqrt{\frac{A}{EOA} - 1} - \alpha\left[\left(\frac{A}{EOA}\right)^{\beta} - 1\right]^{\gamma}. \tag{9}$$

It is straightforward to verify that L_{23} is zero if $EOA = A$. Because L_{23} may not be infinite, it is meaningful to postulate that $(L_{23}/\sqrt{A})$ must converge towards a strictly positive constant when A/EOA tends towards $+\infty$, i.e. when the stenosis becomes more and more severe ($EOA \to 0$). This essential postulate leads to the unique following solution (see Appendix A):

$$\alpha = 2\pi, \quad \beta = 1/2 \quad \text{and} \quad \gamma = 1. \tag{10}$$

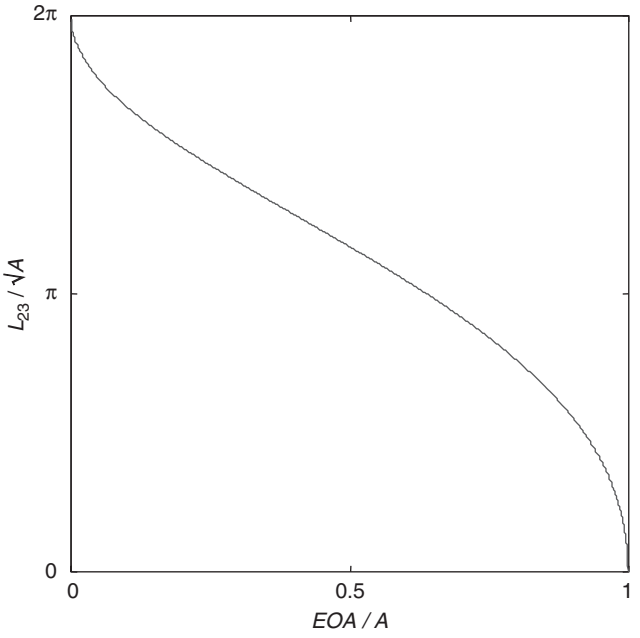

Fig. 2. Normalized recovery length as a function of normalized EOA. A is the aortic cross-sectional area.

Finally, the recovery length can be expressed as

$$L_{23} = 2\pi\sqrt{A}\left(\sqrt{\frac{A}{EOA} - 1} - \sqrt{\frac{A}{EOA}} + 1\right). \tag{11}$$

Fig. 2 illustrates the dimensionless recovery length $(L_{23}/\sqrt{A})$ as a function of the dimensionless EOA (EOA/A). Using Eqs. (7) and (10), one finally obtains:

$$TPG_{max} = \frac{1}{2}\rho Q^2\left(\frac{1}{EOA^2} - \frac{1}{A^2}\right) + 2\pi\rho\frac{\partial Q}{\partial t}\left(\frac{1}{\sqrt{EOA}} - \frac{1}{\sqrt{A}}\right). \tag{12}$$

For comparison, TPG_{net} is written as (see (Garcia et al., 2005b) for details):

$$TPG_{net} = \frac{1}{2}\rho Q^2\left(\frac{1}{EOA} - \frac{1}{A}\right)^2 + 2\pi\rho\frac{\partial Q}{\partial t}\sqrt{\frac{1}{EOA} - \frac{1}{A}}. \tag{13}$$

The expression of TPG_{max} given by Eq. (12) has been validated in vivo as described hereafter.

3. Methods: in vivo validation of the TPG_{max} equation

3.1. In vivo experiments

The animal protocol has been previously described in detail (Garcia et al., 2003; Kadem et al., 2005). A supravalvular AS was created in 19 pigs using umbilical tape tightened around the aorta ~2 cm downstream from the aortic valve annulus. The pressure measurements were performed using a Millar catheter (customized model, Millar Instruments) with a distal ($P_1 = P_{LV}$), intermediary ($P_2 = P_{VC}$), and proximal ($P_3 = P_A$) sensor. The P_1 sensor was located ~1 cm upstream from the stenosis. The P_2 was positioned at the level of the vena contracta. The P_3 sensor, located at 4 cm of the intermediary sensor (P_2), was used to measure the aortic pressure after recovery. Cardiac output was measured using an ultrasonic flowmeter (T206, Transonic Systems), with the probe positioned around the main pulmonary artery. The three pressure signals were simultaneously recorded using a sampling frequency of 400 Hz. The systolic trans-stenotic pressure gradients were calculated as follows: $TPG_{max} = P_1 - P_2$ ($= P_{LV} - P_{VC}$) and $TPG_{net} = P_1 - P_3$ ($= P_{LV} - P_A$). Doppler echocardiographic measurements were performed with a Sonos 5500. Doppler EOA was calculated using the standard continuity equation. The diameter of the ascending aorta was measured at ~2 cm downstream of the stenosis by bi-dimensional echocardiography. The cross-sectional area A was calculated assuming a circular shape. These measurements were obtained under different grades of stenosis severity (1–3 grades per pig). In total, 33 complete series of acquisitions were obtained. It should be noted that the normal native aortic valve does not affect the flow through the supravalvular stenosis since the valve is widely open during systole.

3.2. Determination of the instantaneous transvalvular flow rate

The instantaneous transvalvular flow rate (Q) was necessary to predict TPG_{max} (see Eq. (12)). However, only the pulmonary flow waveform was measured. The transvalvular flow waveform was therefore determined from the continuous-wave Doppler spectrum measured in the trans-stenotic flow jet: the respective envelopes of three spectra were semi-automatically extracted using a Matlab (MathWorks, Inc.) programme and their average was used as a substitute of the Q waveform (Fig. 3). This approach is valid because the geometric area of the stenosis did not significantly change during systole. Then, the amplitude of the reconstructed flow signal was adjusted to match the time-averaged pulmonary flow (= cardiac output).

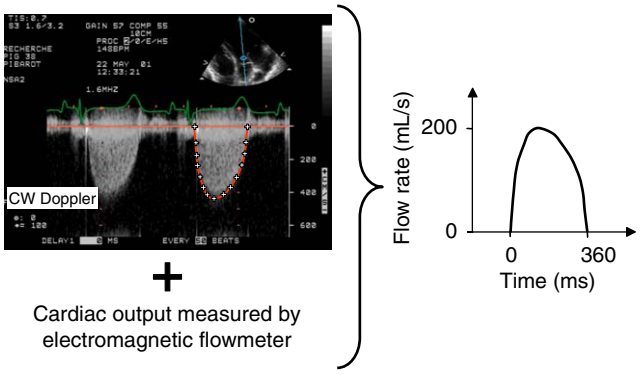

Fig. 3. Determination of the transvalvular flow waveform from the envelope of the continuous-wave (CW) Doppler spectrum and cardiac output measured by electromagnetic flowmeter. See Section 3.2 for details.

3.3. Comparison between measured and predicted TPG_{max}

As shown by Eq. (12), TPG_{max} is dependent upon $\partial Q/\partial t$. However, it is difficult to obtain an accurate $\partial Q/\partial t$ waveform from Doppler signal, especially at the ejection onset. We therefore chose to predict TPG_{max} from Q^2 and TPG_{net}, rather than from Q^2 and $\partial Q/\partial t$ (as in Eq. (12)). Indeed, by means of Eqs. (12) and (13), TPG_{max} can be rewritten as follows:

$$\mathrm{TPG_{max}} = \frac{1}{2}\rho\frac{a_1 b_2 - a_2 b_1}{b_2}Q^2 + \frac{b_1}{b_2}\mathrm{TPG_{net}}$$
$$\text{where}\begin{cases} b_1 = 1/\sqrt{\mathrm{EOA}} - 1/\sqrt{A} \\ b_2 = \sqrt{1/\mathrm{EOA} - 1/A} \\ a_1 = 1/\mathrm{EOA}^2 - 1/A^2 \\ a_2 = (1/\mathrm{EOA} - 1/A)^2. \end{cases} \quad (14)$$

EOA was determined by Doppler echocardiography (see Section 3.1) and also by catheter with the use of the mean systolic expression of Eq. (13):

$$\mathrm{EOA} = \left(\frac{1}{A} + \sqrt{\frac{2}{\rho}\frac{\overline{\mathrm{TPG_{net}}}}{\overline{Q^2}}}\right)^{-1}. \quad (15)$$

3.4. Analysis of the results

TPG_{max} was predicted from Eq. (14) with the use of either Doppler or catheter EOA (Eq. (15)). Total relative errors between the measured and predicted instantaneous TPG_{max} were calculated as: $|TPG_{measured} - TPG_{estimated}| \div |TPG_{measured}| \times 100$, where $|\cdot|$ represents the vectorial

1-norm. Mean absolute errors were calculated as: $|TPG_{measured} - TPG_{estimated}|/N$, where N represents the vector length. Doppler and catheter EOAs were compared using a linear regression and the Bland–Altman method (Bland and Altman, 1986).

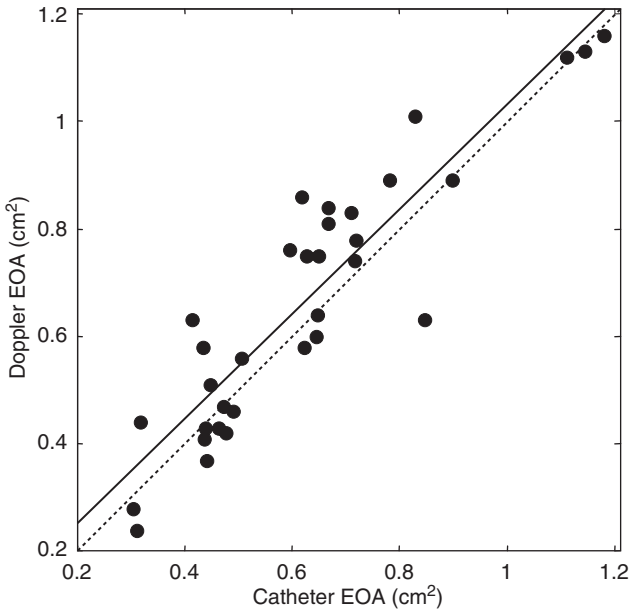

Fig. 4. Doppler EOA versus catheter EOA ($n = 33$). The dotted line is the identity line. The solid line is the regression line.

4. Results

4.1. Doppler versus catheter EOAs

The Doppler EOA ranged from 0.24 to 1.16 cm^2 and the catheter EOA from 0.30 to 1.18 cm^2. The equation of the regression line linking Doppler and catheter EOAs was $y = 0.97x + 0.06$ with a coefficient of determination of $r^2 = 0.83$ (Fig. 4). The mean ($\pm$SD) of the difference (Doppler EOA–catheter EOA) was $0.04 \pm 0.1\ cm^2$. No correlation was found between the differences and catheter EOA ($r^2 < 0.01$). Our results thus suggest that there was a very good concordance between Doppler and catheter EOAs and that their differences behaved randomly.

4.2. Predicted versus measured TPG_{max}

Overall there was a very good concordance between measured and predicted TPG_{max} when using catheter EOA (Fig. 5), which validates Eq. (14). Total relative error ranged between 3.6% and 26% (Fig. 6) and was on average $9.4 \pm 4.9\%$ (median = 8.6%). Mean absolute

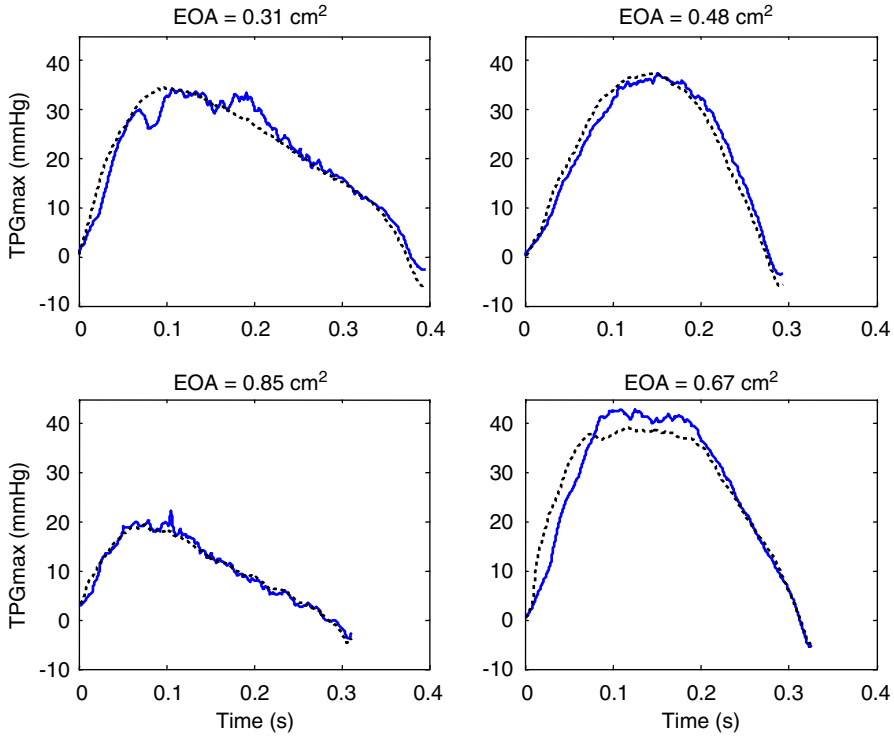

Fig. 5. Predicted (dotted curves) versus measured (solid curves) TPG_{max}. These examples correspond to the four median results in terms of total relative error (white dots in left panel, Fig. 6). Here, total relative error is around 8.5%.

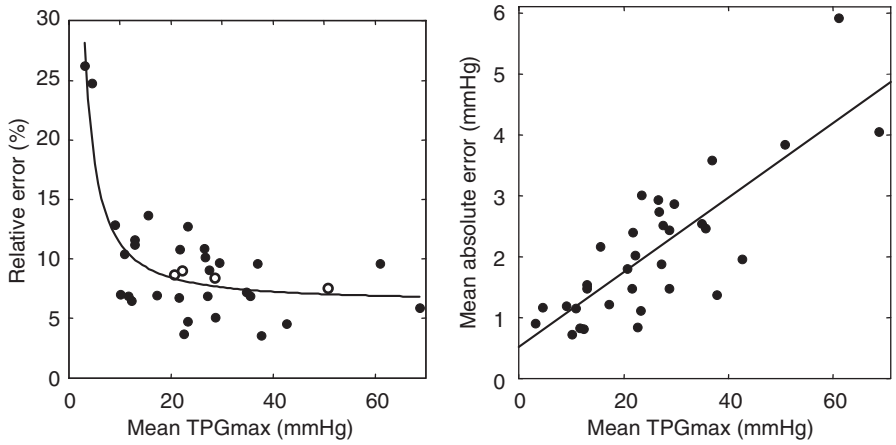

Fig. 6. Total relative errors (left panel) and mean absolute errors (right panel), between predicted and measured TPG_{max}, as a function of the mean systolic measured TPG_{max}. White dots in the left panel correspond to the curves of Fig. 5.

error ranged between 0.7 and 5.9 mmHg (Fig. 6) and was on average 2.1 ± 1.1 mmHg (median = 1.9 mmHg). When the mean TPG_{max} was less than 20 mmHg, relative error was greater than 10%. Nevertheless, in this particular range, the mean absolute error remained around 1.5 mmHg only (Fig. 6). When TPG_{max} was predicted using Doppler EOA, relative and absolute errors were $20 \pm 11\%$ (median = 18%) and 4.5 ± 2.9 (median = 4.0) mmHg, respectively. Hence, although there was a very good concordance between Doppler and catheter EOAs, TPG_{max} estimated when using Doppler EOA did not predict measured TPG_{max} as well as with catheter EOA. This suggests that the proposed equations are sensitive to error measurements in EOA.

5. Discussion

The mean systolic values of TPGs are commonly utilized during clinical examination to evaluate the severity of AS, and they can be determined either by cardiac catheterization or by Doppler echocardiography. Since Doppler echocardiography uses the velocity measured in the vena contracta, it provides the mean TPG_{max} as given by the simplified Bernoulli equation resulting from Eq. (3). In contrast, catheterization measures the recovered pressure at some distance from the vena contracta and thus gives the mean TPG_{net} which may be expressed from Eq. (13) as:

$$\overline{TPG_{net}} = \frac{1}{2}\rho\overline{Q^2}\left(\frac{1}{EOA} - \frac{1}{A}\right)^2. \tag{16}$$

Because the amount of "overestimation" of Doppler gradients compared to catheter gradients may be clinically significant in patients with moderate or severe stenosis and a relatively small aortic cross-sectional area, mean systolic TPG_{max} and TPG_{net} have been widely studied (Baumgartner et al., 1999; Voelker et al., 1992). However, few investigations were carried out on instantaneous TPG_{net} and, to our knowledge, none on instantaneous TPG_{max}. Recently, we have proposed an explicit analytic expression for the instantaneous TPG_{net} (Garcia et al., 2005b). To pursue this investigation of the transvalvular hemodynamics, we now derived the analytic equation of instantaneous TPG_{max}. Some important features and potential clinical implications of such a model are discussed below.

5.1. Generalization of TPG_{net} and TPG_{max}

In the present study, we assumed that LVOT and aortic cross-sectional areas were similar. However, in patients with AS, these areas are significantly different: from a database of 1261 patients who underwent an echocardiographic evaluation at the Quebec Heart Institute, LVOT area was on average $3.6 \pm 0.8\,cm^2$ whereas aortic area measured at the sinotubular junction was $7.0 \pm 3.4\,cm^2$. Nonetheless, we showed that the contribution of the LVOT area in TPG_{net} is less than 10% in most of the patients (Garcia et al., 2005b). Moreover, it is well established that the dimension and geometry of the flow downstream of the vena contracta has a minimal influence on the flow characteristics upstream from the vena contracta (Garcia et al., 2004; Gurevich, 1965; Ward-Smith, 1980). Hence TPG_{max} and TPG_{net} can be generalized as follows:

$$TPG_{max} = \frac{1}{2}\rho Q^2\left(\frac{1}{EOA^2} - \frac{1}{A_{LV}{}^2}\right) + 2\pi\rho\frac{\partial Q}{\partial t}\left(\frac{1}{\sqrt{EOA}} - \frac{1}{\sqrt{A_{LV}}}\right), \tag{17}$$

$$TPG_{net} = \frac{1}{2}\rho Q^2\left(\frac{1}{EOA} - \frac{1}{A_A}\right)^2 + 2\pi\rho\frac{\partial Q}{\partial t}\sqrt{\frac{1}{EOA} - \frac{1}{A_A}}, \tag{18}$$

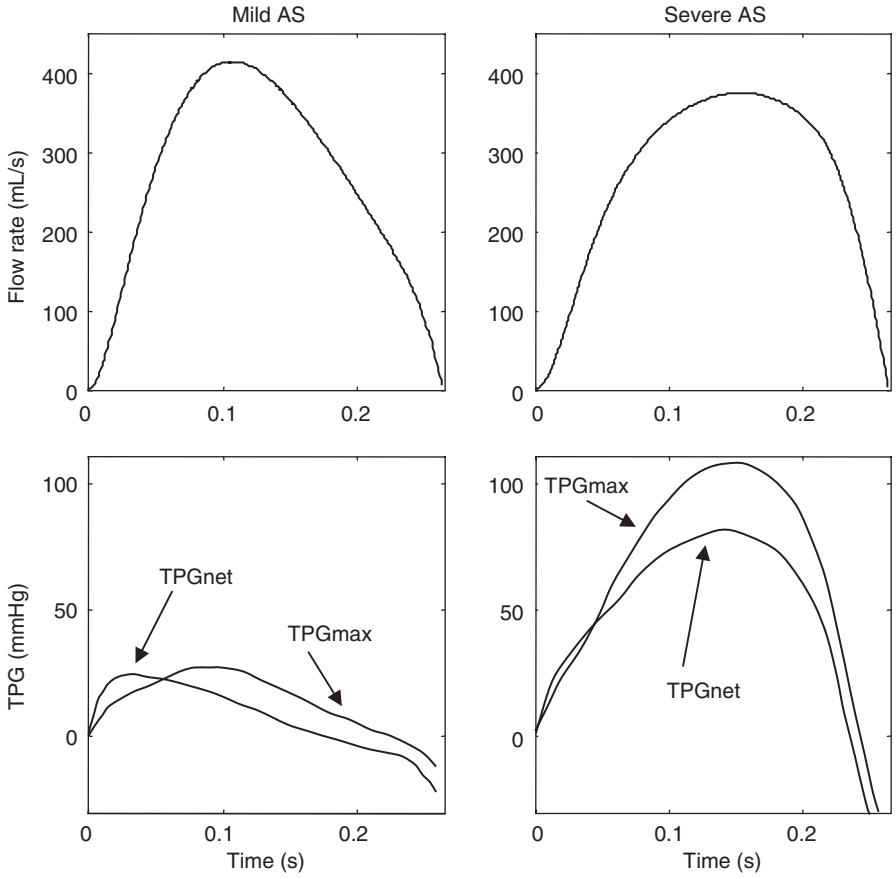

Fig. 7. Simulated TPG_{net} and TPG_{max} using the V^3 model for mild (EOA = 1.5 cm^2) and severe (EOA = 0.7 cm^2) AS. Stroke volume is 70 mL, and heart rate is 70 bpm. Note that TPG_{max} is lower than TPG_{net} at the very beginning of ejection.

where A_{LV} and A_A are the respective cross-sectional areas of the LVOT and the ascending aorta at the sinotubular junction (Fig. 1).

5.2. TPG_{max} is not always maximal!

TPG_{max} is called this way because, when averaging throughout systole, it is indeed the maximal transvalvular pressure gradient, as could be easily demonstrated from Eqs. (3) and (16). However, at the very beginning of LV ejection, Q^2 is negligible compared to $\partial Q/\partial t$ so that TPG_{max} and TPG_{net} are essentially governed by the local inertia. In that case, $TPG_{net}(t) > TPG_{max}(t)$ (Fig. 7). Hence, the pressure at the vena contracta (location 2, Fig. 1) is therefore higher than the recovered aortic pressure (location 3, Fig. 1) at the onset of LV ejection (Fig. 8).

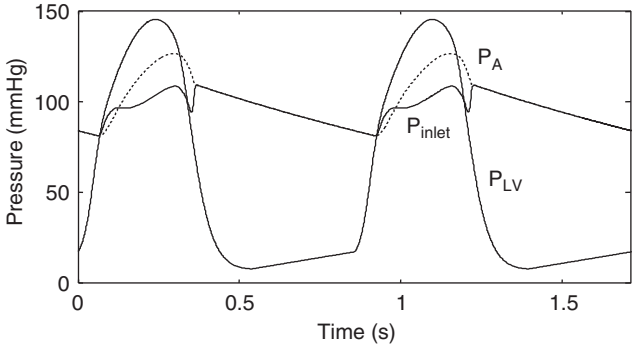

Fig. 8. Pressure waveforms obtained with the V^3 model upgraded with Eq. (17) and (19). P_{LV} = left ventricular pressure, P_{inlet} = left coronary inlet pressure ($= P_{VC}$), P_A = aortic pressure. In this example, a normotensive condition was simulated and stroke volume = 70 mL, EOA = 1 cm^2, $A_{LV} = 3.5$ and $A_A = 7$ cm^2.

5.3. Recovery length

The recovery length (L_{23}, Fig. 2) can be expressed as a function of the aortic cross-sectional area and EOA alone, as shown by Eq. (11). In this animal study, aortic area was on average 2.4 ± 0.5 cm^2 and catheter EOA ranged from 0.3 to 1.2 cm^2. According to Eq. (11), L_{23} therefore ranged from 5.5 to 8 cm approximately, which is higher than the distance separating P_3 and P_2 sensors (4 cm, see methods) in the catheter used for the experiments. But, downstream of vena contracta, static pressure increases rapidly in the first ~5 cm (Sung et al., 1997). It should also be noted that L_{23} is not flow-dependent because we assumed that the flow pattern was dependent upon EOA and A only. This is probably true for high flow rates but should be verified for low flow rates.

5.4. Integration of TPG_{max} in the V^3 model and future investigations

The present study completes the comprehensive description of the aortic valve hemodynamics and this may have several important clinical implications. Indeed we have recently developed and validated a mathematical model (V^3 model) describing the ventricular–valvular–vascular interaction (Garcia et al., 2005a) which allows simulating left heart and vascular hemodynamics under many pathophysiologic conditions (hypertension and/or AS and/or LV failure). Integrating Eq. (17) of TPG_{max} in the V^3 model will now permit simulating the static pressure within the vena contracta and consequently the left coronary inlet pressure. Thus, to summarize, left coronary inlet pressure may be written as

$$\begin{aligned} P_{inlet}(t) &= P_{LV}(t) - TPG_{max}(t) \quad \text{during systole,} \\ P_{inlet}(t) &= P_A(t) \quad \text{during diastole.} \end{aligned} \tag{19}$$

This implies that TPG_{max} may have a critical effect on the left coronary circulation as previously observed in patients (Jin, 2004; Omran et al., 1996; Rajappan et al., 2002; Tamborini et al., 1996). Combining the V^3 model upgraded with the new TPG_{max} equation (Fig. 8) with the lumped model of left coronary circulation developed by Judd and Mates (1991) and Mates and Judd (1993) will permit to further examine the impact of AS on coronary blood flow (CBF) and, more specifically, on coronary flow reserve (CFR). According to the Judd's model, the mean CBF is essentially governed by $(P_{inlet} - \frac{1}{2}P_{LV})$. As the severity of AS increases, it appears a substantial increase of P_{LV} in combination with a lower pressure zone at the coronary inlet. This tends to significantly diminish systolic CBF which represents, under normal conditions, 20–30% of total CBF. To compensate for this loss of CBF, autoregulatory coronary vasodilation occurs to maintain an adequate myocardial perfusion to the detriment of the CFR. Thus, the impairment of the systolic CBF may greatly affect the CFR. This has been previously reported in patients with AS by Hongo et al. (Hongo et al., 1993) who found that CFR positively correlates to the proportion of systolic CBF. Thus, as the severity of AS increases, it is very likely that CFR decreases due to the increase of both TPG and P_{LV}. Moreover, because the difference between TPG_{max} and TPG_{net} may be as high as 30 mmHg with severe AS (Fig. 7), it is essential to use P_{inlet}, yielded by Eq. (19), and not P_A when simulating the systolic coronary inlet pressure.

6. Limitations of the study

The derivation of the analytical expression of TPG_{max} necessitated the same essential hypotheses used previously for TPG_{net} (Garcia et al., 2005b): (1) ideal flow upstream from the vena contracta, (2) flat velocity profiles in the through-flow, (3) fixed flow geometry throughout systole and (4) equality of LVOT and ascending aorta cross-sectional areas. Hypotheses 1 and 2 are commonly applied in some models of flowmetering devices even if some vortices may appear proximal to the vena contracta (Miller, 1996; Munson et al., 1994; Ward-Smith, 1980). Moreover, because the transvalvular flow is not rectilinear nor axisymmetric, irregular velocity profiles have been reported both in LVOT and in ascending aorta (Haugen et al., 2000; Segadal and Matre, 1987). We also postulated that EOA is constant throughout ejection. Whereas this hypothesis is adequate in normal and mildly or moderately stenotic aortic valves, it has been reported that EOA may vary during ejection in patients with severely calcified valves (Arsenault et al., 1998; Beauchesne et al., 2003). Hence, further studies should be necessary to evaluate the accuracy of the model in patients with various degrees of AS and/or valve leaflet calcification.

Acknowledgements

This work was supported by an operating grant from the Canadian Institutes of Health Research (MOP-10929). The authors thank Lynn Atton, Guy Noël, Justin Robillard, Guy Rossignol, Claudia Jones and Martine Lauzier for their technical assistance, and Christopher Hall for his suggestions.

Appendix A

One seeks the values of the strictly positive constants α, β and γ so that:

$$\lim_{(A/EOA)\to+\infty} \left(\frac{L_{23}}{\sqrt{A}}\right) = \text{constant} > 0. \tag{A.1}$$

We define the variable $X = (A/EOA - 1)$. Thus, it follows from Eq. (9) that:

$$L_{23}/\sqrt{A} = 2\pi X^{1/2} - \alpha[X^{\beta}(1 + X^{-1})^{\beta} - 1]^{\gamma}. \tag{A.2}$$

When X tends towards $+\infty$, one obtains:

$$\begin{aligned} L_{23}/\sqrt{A} &\approx 2\pi X^{1/2} - \alpha(X^{\beta} + \beta X^{\beta-1} - 1)^{\gamma} \\ &\approx 2\pi X^{1/2} - \alpha X^{\beta\gamma}(1 + \beta X^{-1} - X^{-\beta})^{\gamma} \\ &\approx 2\pi X^{1/2} - \alpha X^{\beta\gamma}(1 + \beta\gamma X^{-1} - \gamma X^{-\beta}) \\ &\approx 2\pi X^{1/2} - \alpha X^{\beta\gamma} - \alpha\beta\gamma X^{\beta\gamma-1} + \alpha\gamma X^{\beta\gamma-\beta}. \end{aligned} \tag{A.3}$$

Because $\alpha X^{\beta\gamma} + \alpha\beta\gamma X^{\beta\gamma-1} - \alpha\gamma X^{\beta\gamma-\beta} \approx \alpha X^{\beta\gamma}$ when X tends towards $+\infty$, postulate (A.1) is true if, and

only if:

$$\lim_{X\to+\infty}(2\pi X^{1/2}-\alpha X^{\beta\gamma}) = 0 \text{ and } \lim_{X\to+\infty}(-\alpha\beta\gamma X^{\beta\gamma-1}+\alpha\gamma X^{\beta\gamma-\beta}) = \text{constant}>0 \quad (A.4)$$

what necessarily yields:

$$\alpha=2\pi, \beta\gamma=1/2 \text{ and } \lim_{X\to+\infty}(-\pi X^{-1/2}+2\pi\gamma X^{1/2-1/(2\gamma)}) = \text{constant}>0 \quad (A.5)$$

and the unique condition for the limit in (A.5) to converge towards a strictly positive constant is $\gamma=1$, such that the corresponding constant is 2π and $\beta=\frac{1}{2}$. Finally,

$$\alpha=2\pi, \beta=1/2 \text{ and } \gamma=1. \quad (A.6)$$

References

Arsenault, M., Masani, N., Magni, G., Yao, J., Deras, L., Pandian, N., 1998. Variation of anatomic valve area during ejection in patients with valvular aortic stenosis evaluated by two-dimensional echocardiographic planimetry: comparison with traditional Doppler data. Journal of the American College of Cardiology 32, 1931–1937.

Baumgartner, H., Stefenelli, T., Niederberger, J., Schima, H., Maurer, G., 1999. Overestimation of catheter gradients by Doppler ultrasound in patients with aortic stenosis: a predictable manifestation of pressure recovery. Journal of the American College of Cardiology 33, 1655–1661.

Beauchesne, L.M., deKemp, R., Chan, K.L., Burwash, I.G., 2003. Temporal variations in effective orifice area during ejection in patients with valvular aortic stenosis. Journal of the American Society of Echocardiography 16, 958–964.

Bland, J.M., Altman, D.G., 1986. Statistical methods for assessing agreement between two methods of clinical measurement. Lancet 1, 307–310.

Braunwald, E., Sarnoff, S.J., Case, R.B., Stainsby, W.N., Welch Jr., G.H., 1958. Hemodynamic determinants of coronary flow: effect of changes in aortic pressure and cardiac output on the relationship between myocardial oxygen consumption and coronary flow. American Journal of Physiology 192, 157–163.

Garcia, D., Dumesnil, J.G., Durand, L.G., Kadem, L., Pibarot, P., 2003. Discrepancies between catheter and Doppler estimates of valve effective orifice area can be predicted from the pressure recovery phenomenon: practical implications with regard to quantification of aortic stenosis severity. Journal of the American College of Cardiology 41, 435–442.

Garcia, D., Pibarot, P., Landry, C., Allard, A., Chayer, B., Dumesnil, J.G., Durand, L.G., 2004. Estimation of aortic valve effective orifice area by Doppler echocardiography: effects of valve inflow shape and flow rate. Journal of the American Society of Echocardiography 17, 756–765.

Garcia, D., Barenbrug, P.J., Pibarot, P., Dekker, A.L., van der Veen, F.H., Maessen, J.G., Dumesnil, J.G., Durand, L.G., 2005a. A ventricular–vascular coupling model in presence of aortic stenosis. American Journal of Physiology Heart and Circulatory Physiology 288, H1874–H1884.

Garcia, D., Pibarot, P., Durand, L.G., 2005b. Analytical modeling of the instantaneous pressure gradient across the aortic valve. Journal of Biomechanics 38, 1303–1311.

Gurevich, M.I., 1965. Theory of Jets in Ideal Fluids. Academic Press, New York and London.

Haugen, B.O., Berg, S., Brecke, K.M., Samstad, S.O., Slordahl, S.A., Skjaerpe, T., Torp, H., 2000. Velocity profiles in mitral blood flow based on three-dimensional freehand colour flow imaging acquired at high frame rate. European Journal of Echocardiography 1, 252–256.

Hoffman, J.I., Spaan, J.A., 1990. Pressure-flow relations in coronary circulation. Physiological Reviews 70, 331–390.

Hongo, M., Goto, T., Watanabe, N., Nakatsuka, T., Tanaka, M., Kinoshita, O., Yamada, H., Okubo, S., Sekiguchi, M., 1993. Relation of phasic coronary flow velocity profile to clinical and hemodynamic characteristics of patients with aortic valve disease. Circulation 88, 953–960.

Jin, X.Y., 2004. Elucidation of cardiac physiology in aortic valve replacement: what should we know? Journal of Heart Valve Disease 13 (Suppl. 1), S70–S75.

Judd, R.M., Mates, R.E., 1991. Coronary input impedance is constant during systole and diastole. American Journal of Physiology 260, H1841–H1851.

Kadem, L., Dumesnil, J.G., Rieu, R., Durand, L.G., Garcia, D., Pibarot, P., 2005. Impact of systemic hypertension on the assessment of aortic stenosis. Heart 91, 354–361.

Mates, R.E., Judd, R.M., 1993. Models for coronary pressure-flow relationships. In: Sideman, S., Beyar, R. (Eds.), Interactive Phenomena in the Cardiac System. Plenum Press, New York, pp. 153–161.

Miller, D.S., 1996. Internal Flow Systems. BHR, Bedford.

Munson, B.R., Young, D.F., Okiishi, T.H., 1994. Viscous flow in pipes. In: Fundamentals of Fluid Mechanics, second ed. John Wiley & Sons, Inc., New York, pp. 455–547.

Omran, H., Fehske, W., Rabahieh, R., Hagendorff, A., Luderitz, B., 1996. Relation between symptoms and profiles of coronary artery blood flow velocities in patients with aortic valve stenosis: a study using transoesophageal Doppler echocardiography. Heart 75, 377–383.

Rajappan, K., Rimoldi, O.E., Dutka, D.P., Ariff, B., Pennell, D.J., Sheridan, D.J., Camici, P.G., 2002. Mechanisms of coronary microcirculatory dysfunction in patients with aortic stenosis and angiographically normal coronary arteries. Circulation 105, 470–476.

Segadal, L., Matre, K., 1987. Blood velocity distribution in the human ascending aorta. Circulation 76, 90–100.

Sung, H.W., Yu, P.S., Hsu, C.H., Hsu, J.C., 1997. Can cardiac catheterization accurately assess the severity of aortic stenosis? An in vitro pulsatile flow study. Annals of Biomedical Engineering 25, 896–905.

Tamborini, G., Barbier, P., Doria, E., Galli, C., Maltagliati, A., Ossoli, D., Susini, G., Pepi, M., 1996. Influences of aortic pressure gradient and ventricular septal thickness with systolic coronary flow in aortic valve stenosis. American Journal of Cardiology 78, 1303–1306.

Tornos, P., 2001. New aspects in aortic valve disease. Revista Espanola de Cardiologia 54, 17–21.

Voelker, W., Reul, H., Stelzer, T., Schmidt, A., Karsch, K.R., 1992. Pressure recovery in aortic stenosis: an in vitro study in a pulsatile flow model. Journal of the American College of Cardiology 20, 1585–1593.

Ward-Smith, A.J., 1980. Internal Fluid Flow. The Fluid Dynamics of Flow in Pipes and Ducts. Clarendon Press, Oxford.